# Dynamic Crack Propagation along Elastic Interfaces in Double Cantilever Beams under High Loading Rates

Tianyu Chen[1]; Bo Yuan[2]; Christopher M. Harvey, Ph.D.[3]; Kun Zhang[4]; Simon Wang[5]; Vadim V. Silberschmidt[6]; and Bingchen Wei[7]

**Abstract:** The dynamic mode-I energy release rate of cracks propagating along elastic interfaces in double cantilever beams under high loading rates is derived analytically for the first time by accounting for structural vibration, wave propagation, and the Doppler effect along with the assumption of crack tip energy conservation. The developed theory can be used to study the "stick-slip" crack propagation behavior commonly observed in experiments, a progression of crack initiation, propagation, arrest, and reinitiation. In addition, the developed theory can be applied to measure crack initiation toughness as well as crack arrest toughness. The developed theory is verified against results from finite-element-method simulations of two experimental cases under high loading rates, demonstrating the excellent ability of the developed theory in capturing the crack propagation behavior as well as the ability in assessing dynamic mode-I energy release rate. **DOI: 10.1061/(ASCE)AS.1943-5525.0001418.** 

**Author keywords:** Beam dynamics; Double cantilever beams; Dynamic mode-I energy release rate; Propagating crack; Elastic interface.



## Introduction

Double cantilever beams (DCBs) are widely used to study the mode-I fracture behavior of carbon fiber–reinforced plastics (CFPRs) and adhesives as well as to measure the fracture toughness for further design critical values. In the quasi-static loading regime, the theory for DCBs was well developed, and standardized test methods were established, such as ASTM D5528 (ASTM 2016) for mode-I interlaminar fracture toughness of CFPRs and ISO 25217 (ISO 2009) for mode-I fracture toughness of structural adhesives. Note that all these standardized tests are for crack initiation toughness (CIT).

In the dynamic loading regime, for stationary cracks, the dynamic effect was only investigated by the kinetic energy of quasi-static motion without consideration of structural vibrations or wave propagations (Smiley and Pipes 1987; Blackman et al. 1996). It was not until the authors' recent studies (Chen et al. 2020a, b, c, d, 2021b) that structural vibration and flexural wave propagation were incorporated explicitly to study the dynamic effect and crack driving force. An accurate solution for the dynamic energy release rate (ERR) was given, and therefore, the CIT value can be determined accurately from experimental measurements. For propagating cracks in DCBs under high loading rates, the crack propagates in a "stick-slip" fashion (Blackman et al. 1995; Friedrich et al. 1989; Kanninen 1974; Kanninen et al. 1977; Sun et al. 2008; Davidson and Anthony 2012; Davidson et al. 2012), that is, with nonsmooth crack propagation as a mixture of stable growth, fast unstable growth, and arrest. Accordingly, the crack arrest toughness (CAT) should be determined as a lower bound to maintain a propagating crack once the crack starts to propagate. It seems that currently the only analytical solution to study a propagating crack in DCBs was from Blackman et al. (1996), but their solution was only for steady-state crack propagation and cannot be used to study the crack arrest phenomenon nor to predict the CAT value.

Based on the authors' previously developed analytical theory for stationary cracks on elastic foundations (Chen et al. 2020b) under high loading rates and the developed technique (Chen et al. 2020a) of crack tip energy conservation to address moving boundaries as the crack propagates, the theory of dynamic crack propagation along an elastic interface in DCBs is developed in this paper. The main achievement of this study is the analysis of the fracture behavior of propagating cracks along linear elastic interfaces, extending the authors' previous publications (Chen et al. 2020a, b) for stationary cracks or cracks at rigid interfaces. To the best

[1]Postdoctoral Researcher, Key Laboratory of Microgravity (National Microgravity Laboratory), Institute of Mechanics, Chinese Academy of Sciences, Beijing 100190, China (corresponding author). ORCID: https://orcid.org/0000-0001-6250-7593. Email: chentianyu@imech.ac.cn

[2]Postdoctoral Researcher, Dept. of Energy and Power Engineering, Tsinghua Univ., Beijing 100084, China. Email: yuanbo11@mail.tsinghua.edu.cn

[3]Senior Lecturer, Dept. of Aeronautical and Automotive Engineering, Loughborough Univ., Loughborough LE11 3TU, UK; School of Mechanical and Equipment Engineering, Hebei Univ. of Engineering, Handan 056038, China. ORCID: https://orcid.org/0000-0003-2179-4711. Email: c.m.harvey@lboro.ac.uk

[4]Associate Professor, Key Laboratory of Microgravity (National Microgravity Laboratory), Institute of Mechanics, Chinese Academy of Sciences, Beijing 100190, China; Professor, School of Engineering Science, Univ. of Chinese Academy of Sciences, Beijing 100049, China. Email: zhangkun@imech.ac.cn

[5]Academic Professor, Dept. of Aeronautical and Automotive Engineering, Loughborough Univ., Loughborough LE11 3TU, UK; Professor, School of Mechanical and Equipment Engineering, Hebei Univ. of Engineering, Handan 056038, China. Email: s.wang@lboro.ac.uk

[6]Professor, Wolfson School of Mechanical, Electrical, and Manufacturing Engineering, Loughborough Univ., Loughborough, Leicestershire LE11 3TU, UK. ORCID: https://orcid.org/0000-0003-3338-3311. Email: v.silberschmidt@lboro.ac.uk

[7]Professor, Key Laboratory of Microgravity (National Microgravity Laboratory), Institute of Mechanics, Chinese Academy of Sciences, Beijing 100190, China; Professor, School of Engineering Science, Univ. of Chinese Academy of Sciences, Beijing 100049, China; Center of Materials Science, and Optoelectronics Engineering, Univ. of Chinese Academy of Sciences, Beijing 100049, China. Email: weibc@imech.ac.cn

Note. This manuscript was submitted on October 13, 2021; approved on December 28, 2021; published online on March 16, 2022. Discussion period open until August 16, 2022; separate discussions must be submitted for individual papers. This paper is part of the ***Journal of Aerospace Engineering***, © ASCE, ISSN 0893-1321.

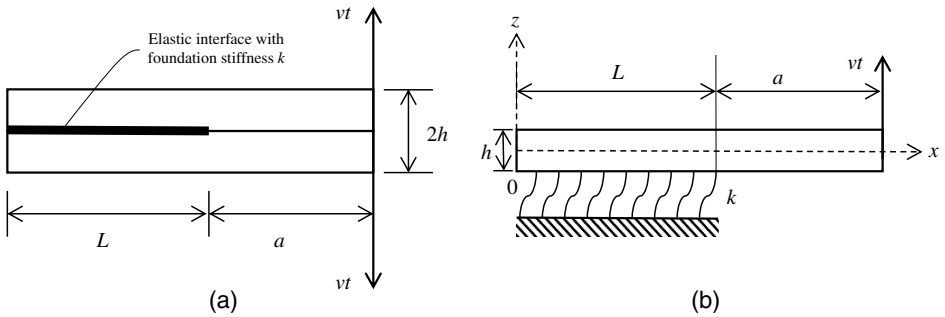


**Fig. 1.** (a) Schematic of DCB specimen; and (b) prescribed coordinate system.



knowledge of the authors, this has not been achieved before analytically. Afforded by the developed theory herein, the "stick-slip" manner of crack propagation can be studied and quantified with respect to the evolution of the dynamic ERR; and the developed theory can also be applied to measure the CIT and CAT values for CFRPs or adhesives in the context of DCB structures.

The theory is developed in the section "Theory" with analytical derivation of dynamic ERR in the section "Dynamic ERR for a Propagating Crack along Elastic Interface," derivation of correction factor for dispersion in the section "Correction Factor for Dispersion," and methods of determining the foundation stiffness in the section "Determination of Foundation Stiffness." In the section "Numerical Verification," the developed analytical theory is verified against published results from the finite-element method (FEM) (Liu et al. 2018), which simulated two experimental results from Blackman et al. (1995, 1996). Conclusions are given in the section "Conclusion."

## Theory

In this section, the dynamic ERR for a propagating crack along an elastic interface in a symmetric DCB is derived analytically. The DCB configuration is shown in Fig. 1(a): the total length of the DCB is $(L + a)$, the crack length is $a$, the uncracked length is $L$, the total thickness is $2h$, the foundation stiffness of the elastic interface is $k$, and $v$ is the applied high constant loading rate with $vt$ being the displacement. In Fig. 1(b), the coordinates are prescribed such that the crack tip is at $x = L$ and deflections take place in the $x$-$z$ plane, denoted as $w^{\mathrm{FD}}(x,t)$ and $w^{\mathrm{FR}}(x,t)$, respectively, for foundation-supported and free beam sections.

According to Chen et al. (2020b), the deflections for foundation-supported and free beam sections are

$$w^{\mathrm{FD}}(x,t) = -v\sum_{i=1}^{\infty}\frac{H_i}{\omega_i}W_i^{\mathrm{FD}}(x)\sin(\omega_i t) + vtF^{\mathrm{FD}}(x) \tag{1}$$

$$w^{\mathrm{FR}}(x,t) = -v\sum_{i=1}^{\infty}\frac{H_i}{\omega_i}W_i^{\mathrm{FR}}(x)\sin(\omega_i t) + vtF^{\mathrm{FR}}(x) \tag{2}$$

where $H_i$ represents the coupling between free vibration and applied opening velocity; $W_i^{\mathrm{FD}}(x)$ and $W_i^{\mathrm{FR}}(x)$ are the $i$th normal mode for free vibration for foundation-supported and free-vibration sections, respectively; and $F^{\mathrm{FD}}(x)$ and $F^{\mathrm{FR}}(x)$ are respective shifting functions. The derivation of these deflections is given in Appendixes I–III, while the derivation of the angular natural frequency $\omega_i$ is given in Appendix II.

For a stationary crack, based on the corrected global approach with account for flexural wave propagation, the dynamic ERR is derived in Chen et al. (2020b) as

$$G = \frac{9EIv^2t^2f_{\mathrm{st}}^{\mathrm{U}}}{ba^4} - \frac{v^2t}{b}\sum_{i=1}^{\infty}(-1)^i\sqrt{\frac{\omega_1}{\omega_i}}H_i^2\frac{d\omega_i}{da}\sin(\omega_i t) \tag{3}$$

where $f_{\mathrm{st}}^{\mathrm{U}}$ is the static ERR reduction factor for linear elastic interface; the derivation of the dynamic ERR is given in Appendix IV.

### Dynamic ERR for a Propagating Crack along Elastic Interface

According to Freund (1990), the dynamic ERR for a propagating delamination is the product of the dynamic ERR for a stationary crack and a factor determined by the crack propagating speed and material properties, which is $(1 - \dot{a}^2/C_0^2)$, where $\dot{a}$ is the crack propagating speed, and $C_0^2 = E/\rho$. Therefore, at crack initiation for a crack length of $a_1$, the dynamic ERR is

$$G_1 = \frac{9EIv^2t^2f_{\mathrm{st}}^{\mathrm{U}}}{ba_1^4}\left(1 - \frac{\dot{a}_1^2}{C_0^2}\right) - \frac{v^2t}{b}\left(1 - \frac{\dot{a}_1^2}{C_0^2}\right)\sum_{i=1}^{\infty}(-1)^i\sqrt{\frac{\omega_1}{\omega_i}}H_i^2\frac{d\omega_i}{da_1}\sin\left[\left(1 - \frac{\dot{a}_1}{C_p^i}\right)\omega_i t\right] \tag{4}$$

where the coefficient of $(1 - \dot{a}_1/C_p^i)$ modifying natural frequency is due to the Doppler effect (Chen et al. 2020a) with $C_p^i$ being the phase speed of the $i$th mode flexural wave; that is, when the $i$th mode flexural wave propagates toward a propagating crack with a crack propagating speed of $\dot{a}_1$, the frequency observed by the crack tip decreases with increasing crack propagating speed.

If the crack propagates from the current crack length of $a_1$ to $a_2$ for a time interval $\Delta t$, a small beam section of length $(a_2 - a_1)$ is formed as shown in Fig. 2. It is worth noting that in Eq. (4), the expression of the first term $G_{\mathrm{st}}^{\mathrm{U}}$ (the ERR component due to strain energy of quasi-static motion, also see Appendix IV) stays the same, but the expression of the second term $G_{\mathrm{vib}}$ (the ERR component due to vibration) needs further investigation since the beam is a kind of highly dispersive waveguide, that is, the wave profile experiences extreme distortion as the flexural waves travel.

The ERR component due to vibration is $G_{\mathrm{vib}} = F_{\mathrm{vib}}(\Omega)/\dot{A}_0$ (Freund 1990), where $F_{\mathrm{vib}}(\Omega)$ is the energy flux into a crack tip contour of $\Omega$, and $\dot{A}_0$ is the rate of crack area increment with $\dot{A}_0 = b\dot{a}$; and combining Eq. (4), the energy flux for crack length $a_1$ is

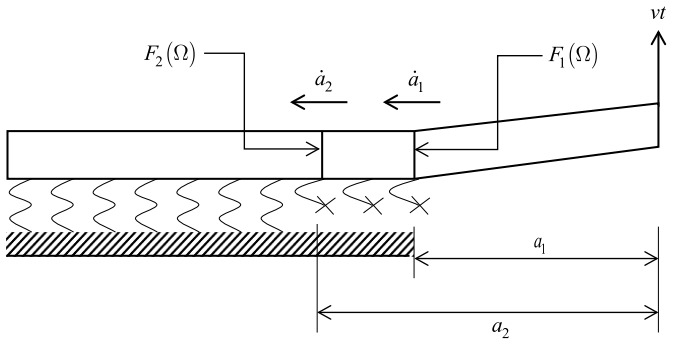


**Fig. 2.** Delamination propagation from $a_1$ to $a_2$ over time interval $\Delta t$ on elastic interface.

$$F_1(\Omega) = b\dot{a}_1 G_{\text{vib}}(a_1) = -v^2 t\dot{a}_1\left(1-\frac{\dot{a}_1^2}{C_0^2}\right)\sum_{i=1}^{\infty}(-1)^i\sqrt{\frac{\omega_1}{\omega_i}}H_i^2\frac{d\omega_i}{da_1}\sin\left[\left(1-\frac{\dot{a}_1}{C_p^i}\right)\omega_i t\right] \tag{5}$$

Note that when the crack propagates from $a_1$ to $a_2$ (even for $a_1 \approx a_2$), the energy flux $F_2(\Omega) \neq F_1(\Omega)$; this is due to the dispersive nature of beams that flexural waves with higher frequencies travel faster and those with lower frequencies travel slower. Therefore, the first mode flexural wave, with the lowest natural frequency, functions like a modulation of the other mode flexural waves. When considering the energy density concept and crack tip energy conservation as laid out in Chen et al. (2020a), the energy flux at the delamination of $a_2$ is

$$F_2(\Omega) = -v^2 t\dot{a}_1\left(1-\frac{\dot{a}_1^2}{C_0^2}\right) \times \sum_{i=1}^{\infty} f_i(-1)^i\sqrt{\frac{\omega_1}{\omega_i}}H_i^2\frac{d\omega_i}{da_1}\sin\left[\left(1-\frac{\dot{a}_1}{C_p^i}\right)\omega_i t\right] \tag{6}$$

where $f_i$ is a correction factor for dispersion given in the section "Correction Factor for Dispersion." Therefore, the ERR component due to vibration for crack length of $a_2$ is

$$G_{\text{vib}}(a_2) = \frac{F_2(\Omega)}{b\dot{a}_2} = -v^2 t\frac{\dot{a}_1}{\dot{a}_2}\left(1-\frac{\dot{a}_1^2}{C_0^2}\right) \times \sum_{i=1}^{\infty} f_i(-1)^i\sqrt{\frac{\omega_1}{\omega_i}}H_i^2\frac{d\omega_i}{da_1}\sin\left[\left(1-\frac{\dot{a}_1}{C_p^i}\right)\omega_i t\right] \tag{7}$$

If $(a_2 - a_1)$ is small and $\dot{a}_2 \approx \dot{a}_1$, Eq. (7) can be written as

$$G_{\text{vib}}(a_2) = \frac{F_2(\Omega)}{b\dot{a}_1} = -v^2 t\left(1-\frac{\dot{a}_1^2}{C_0^2}\right) \times \sum_{i=1}^{\infty} f_i(-1)^i\sqrt{\frac{\omega_1}{\omega_i}}H_i^2\frac{d\omega_i}{da_1}\sin\left[\left(1-\frac{\dot{a}_1}{C_p^i}\right)\omega_i t\right] \tag{8}$$

Note that the condition to derive Eq. (8) as well as Eq. (9) (following) is based on the limiting condition that the propagating crack is about to advance, and in this condition, the changes of the crack length and crack propagating speed are small. Combining the ERR component due to strain energy of quasi-static motion $G_{\text{st}}^{\text{U}}$ [the first term in Eq. (4)], the dynamic ERR for a propagating crack along the elastic interface in DCBs after initiation is

$$G = \frac{9EIv^2t^2f_{\text{st}}^{\text{U}}}{ba^4}\left(1-\frac{\dot{a}^2}{C_0^2}\right) - \frac{v^2t}{b}\left(1-\frac{\dot{a}^2}{C_0^2}\right)\sum_{i=1}^{\infty}(-1)^i f_i\sqrt{\frac{\omega_1}{\omega_i}}H_i^2\frac{d\omega_i}{da}\sin\left[\left(1-\frac{\dot{a}}{C_p^i}\right)\omega_i t\right] \tag{9}$$

Eq. (9) is derived for the plane-stress condition. For the plane-strain condition, the effective Young's modulus of $E/(1-\nu^2)$ should be used.

### Correction Factor for Dispersion

When deriving the ERR component due to vibration, a correction factor for dispersion $f_i$ is introduced to address the dispersive nature of beams in determining ERR. The energy flux modified by this factor gives the accurate assessment of the energy supplied to the crack tip for further crack growth. According to Chen et al. (2020a, b), this correction factor is the ratio between the phase speed of the first mode flexural wave $C_p^1$ and the group speed of the $i$th mode flexural wave $C_g^i$, indicating that the first mode flexural wave functions as the modulation of the other flexural waves, which are determined by the boundary conditions of a newly formed crack increment i.e., the beam section of $(a_2 - a_1)$ shown in Fig. 2. The phase speed of the first mode flexural wave is $C_{\text{p}}^1 = \sqrt{\omega_1}\sqrt[4]{EI/(\rho A)}$ and the group speed of the $i$th mode flexural wave is $C_{\text{g}}^i = 2\sqrt{\omega_i}\sqrt[4]{EI/(\rho A)}$, and, therefore, the correction factor for dispersion is

$$f_i = \frac{C_{\text{p}}^1}{C_{\text{g}}^i} = \frac{1}{2}\sqrt{\frac{\omega_1}{\omega_i}} \tag{10}$$

For the propagating crack shown in Fig. 2, the elastic foundation allows crack tips ($x = a_1$ and $x = a_2$) to rotate and the boundary conditions for the crack increment $(a_2 - a_1)$ are more free than completely fixed-fixed; an elastic foundation, however, does not allow the crack tips to rotate completely free, suggesting the boundary conditions do not achieve a pinned-pinned configuration. Therefore, fixed-fixed and pinned-pinned boundary conditions are two limiting boundary conditions for the newly formed crack increment, between which cases should the correction factor for dispersion $f_i$ be derived. It is, therefore, assumed that $f_i$ can be taken as an average value of those fixed-fixed and pinned-pinned boundary conditions with the value shown in Table 1. Note that for fixed-fixed and pinned-pinned boundary conditions, Eq. (10) becomes $f_i = \lambda_1/(2\lambda_i)$, where $\lambda_i$ is the $i$th eigenvalue, which can

**Table 1.** Correction factor for dispersion for propagating crack

| Mode number | 1 | 2 | 3 | 4 | 5 | $i > 5$ |
|---|---|---|---|---|---|---|
| Fixed-fixed | 0.5 | 0.30115 | 0.21509 | 0.16729 | 0.13687 | $\frac{1.50562}{(2i+1)}$ |
| Pinned-pinned | 0.5 | 0.25 | 0.16667 | 0.125 | 0.1 | $\frac{1}{2i}$ |
| Elastic foundation | 0.5 | 0.257558 | 0.19088 | 0.14615 | 0.11844 | $\frac{5.011i+1}{4i(2i+1)}$ |

be derived by solving the frequency equations of $\cosh(\lambda_i)\cos(\lambda_i) - 1 = 0$ for the fixed-fixed configuration and $\sin(\lambda_i) = 0$ for the pinned-pinned configuration.

### Determination of Foundation Stiffness

The conventional method to determine the foundation stiffness, that is, the Young's modulus, of the resin of CFRPs and adhesives requires a tensile test of "dog bone" specimens as standardized in ISO 527 (ISO 2019) and ASTM D638 (ASTM 2015). However, it is not easy to test adhesives, which could not be made into such a tensile specimen, for instance, the structural adhesive films. Therefore, an alternative method to test DCB configuration to derive foundation stiffness is desirable.

Considering the quasi-static component in deflection in Eq. (2), the external force under quasi-static loading rate is found to be $P = -vtEIF^{\mathrm{FR}(3)}(L + a)$, and then the compliance is $C = vt/P$. Combining Eqs. (30) and (35), this compliance calibration method gives the relationship between compliance and foundation stiffness (represented by $\gamma$) as

$$(2a^3 - 6CEI)\gamma^3 + 6a^2\gamma^2 + 6a\gamma + 3 = 0 \tag{11}$$

where $\gamma = \sqrt[4]{k/(4EI)}$, and, therefore, the foundation stiffness is $k = 4\gamma^4 EI$.

It is suggested by Eq. (11) that the foundation stiffness can be derived by parallel quasi-static tests of the DCB rather than by testing the adhesive directly.

Alternatively, it is worth noting that if the DCB is analyzed by assuming a fixed boundary condition at the crack tip as indicated in ASTM D5528 (ASTM 2016) without using the elastic foundation approach, additional crack length $\Delta$ (Hashemi et al. 1989) is required to compensate for crack tip rotation by regressing multiple compliances against crack lengths. If this additional crack length $\Delta$ is derived, the foundation stiffness $k$ can also be derived by the method given in Chen et al. (2021a), which is

$$\Delta = \frac{1}{\gamma}\sqrt[4]{\frac{(2a^3\gamma^3 + 6a^2\gamma^2 + 6a\gamma + 3)^2}{4(a\gamma + 1)^2}} - a \tag{12}$$

However, thought should be given when using Eq. (12) when it is derived under the plane-stress condition. For the plane-strain condition, the Young's modulus should be replaced by the effective Young's modulus of $E/(1–\nu^2)$) and the unit width should be used to derive foundation stiffness via $k = 4\gamma^4 EI$.

## Numerical Verification

Numerical simulations of a DCB of PEEK/carbon fiber under 6.5 and 10.0 $\mathrm{m\,s^{-1}}$ opening rates in Liu et al. (2018) for experiments in Blackman et al. (1995, 1996) were used to verify the developed theory in the section "Theory," i.e., the analytical solution for Eq. (9) of dynamic ERR for propagating crack along elastic interface. Note that before crack initiation, i.e., a stationary crack, Eq. (3) was employed to calculate the dynamic ERR.

The considered material properties and DCB geometry are listed in Table 2.

Liu et al. (2018) also provided CIT and CAT values for these two cases by parametric studies to match the experimentally derived crack-versus-time curves: in the 6.5 $\mathrm{m\,s^{-1}}$ opening rate case, the CIT was 1,400 $\mathrm{N\,m^{-1}}$ and CAT was 670 $\mathrm{N\,m^{-1}}$; in the 10.0 $\mathrm{m\,s^{-1}}$ case, they were 1,300 $\mathrm{N\,m^{-1}}$ and 300 $\mathrm{N\,m^{-1}}$, respectively. These toughness values were not required to calculate the dynamic ERR employing the theory developed in the section "Theory," they were plotted only in the respective cases for comparison. Note that the CIT and CAT values could not be obtained from the experiments since there was no analytical theory based on dynamics to post-process the experimental data; this is the aim of this study, to develop such a theory. In addition, the numerical solution of ERR computed in Liu et al. (2018) provides the ERR time response in detail, and this is ideal to validate the developed theory.

The foundation stiffness is derived by the quasi-static load-versus-time curve of DCB, that is, Fig. 8(a) in Blackman et al. (1995), which provides a compliance of 1/28,382 m/N. According to Eq. (11), the compliance calibration method gives the foundation stiffness $k = 1.18$ GPa. Alternatively, Eq. (12) can be used with the $\Delta = 3.6$ mm provided in Blackman et al. (1995), giving $k = 0.96$ GPa. The two methods of determining foundation stiffness provide similar results. In the following verifications, $k = 1.18$ GPa is employed.

The crack length-time curves from the FEM simulations in Liu et al. (2018) were employed as the input data to calculate the respective physical quantities and, finally, the ERR was determined by Eq. (9). The detailed implementation is shown in Fig. 3.

1. Numerical verification for DCBs under 6.5 $\mathrm{m\,s^{-1}}$ opening rate

The theoretical solution of dynamic ERR for the DCB test under 6.5 $\mathrm{m\,s^{-1}}$ opening rates was plotted against time in Fig. 4 while the corresponding crack length from Liu et al. (2018) was plotted on the secondary axis.

Generally, the analytical solution shows an excellent ability to capture the fracture behaviors, such as initiation, propagation, arrest, and reinitiation. (1) Initiation: Before the crack starts to propagate, i.e., for the stationary crack, dynamic ERR builds up with respect to time under the applied constant opening rate. When it reaches the CIT value at $t = 1.04$ ms approximately, the crack starts to propagate, (2) Arrest: As the crack propagates, there is a constant drop of the dynamic ERR with its value under CIT, but the crack still propagates until the dynamic ERR comes to the CAT value at about $t = 3.46$ ms. Once the dynamic ERR gets to the CAT value, the crack stops propagating, i.e., crack arrest, and (3) Reinitiation: After crack arrest, with the applied constant opening rate, the dynamic ERR starts to climb up again until it rises to the CIT value at $t = 4.98$ ms, and the crack starts to propagate again.

Apart from the excellent ability to capture the fracture behavior, the developed theory can also be applied to measure the CIT and CAT values. Note that the developed analytical theory gives a slightly higher ERR compared with the FEM result. This is reasonable since the FEM model employed a three-dimensional (3D) formulation with the anisotropic material properties with $E_{11} = 115$ GPa and $E_{22} = 8$ GPa, making the FEM model less stiff than the analytical model with a one-dimensional (1D) plane-strain condition. This gives a higher prediction for the CIT value in the analytical solution, particularly when the crack length is relatively short, i.e., at crack initiation. But as the crack propagates, the

**Table 2.** Material properties and DCB geometry

| Longitudinal modulus | Poisson's ratio | Effective Young's modulus | Thickness | Width | Crack length |
|---|---|---|---|---|---|
| $E_{11} = 115$ GPa | $\nu = 0.28$ | $E_{11}/(1–\nu^2) = 124.78$ GPa | $h = 1.5$ mm | $b = 20$ mm | Taken from Liu et al. (2018) |

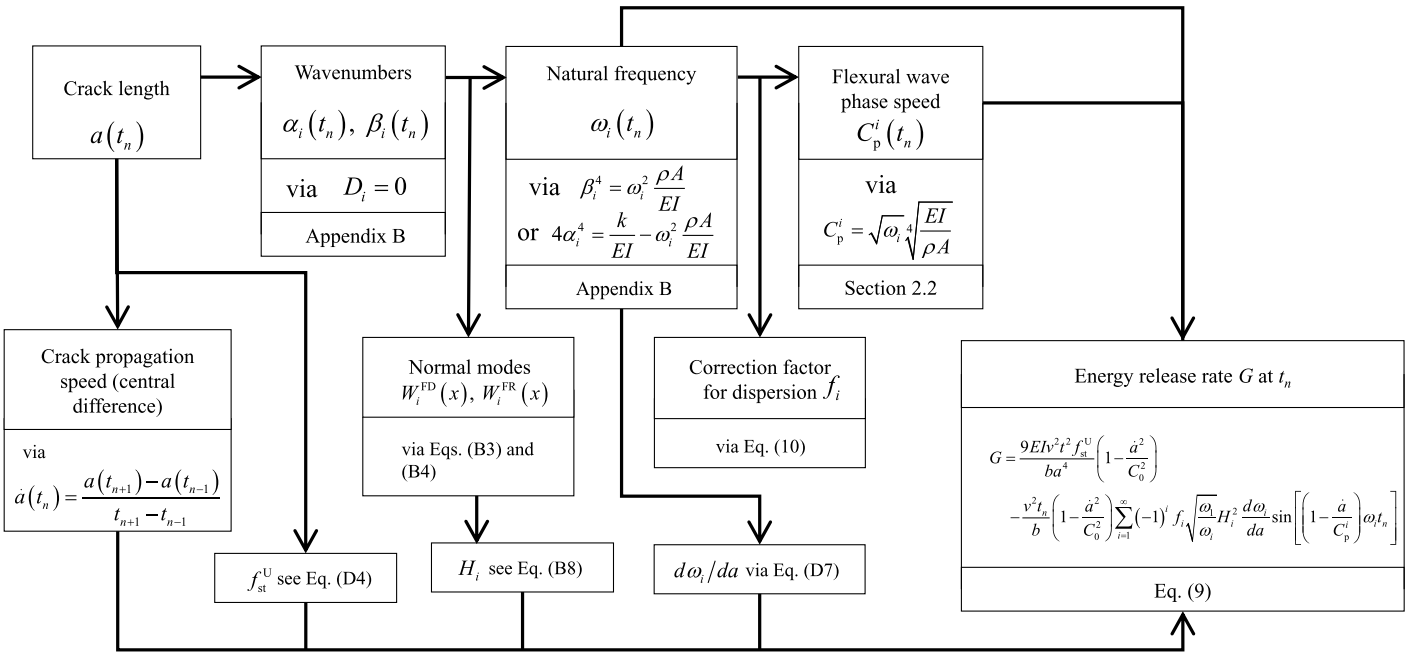


**Fig. 3.** Flowchart of implementation of developed theory to determine ERR.

stiffness of the DCB arm decreases; so, the difference of ERR between the developed theory and FEM result is not significant. The developed theory also gives an accurate prediction of the reinitiation toughness. The relative differences of the CIT values from the developed theory and FEM simulation are 36.8% and 3.2%, respectively, for initiation and reinitiation, while the relative difference for the CAT value is 3.9%.

It is worth noting that before crack initiation, the ERR predicted by the analytical solution in Eq. (3) shows more oscillation than that that predicted with the FEM simulation. This may be due to the fact that the analytical solution considered the energy flux into the crack tip contour locally, but the FEM used an interfacial thick level set (ITLS) formulation to evaluate the ERR nonlocally over a damaged band. This averages out the oscillating nature of stress at the crack tip and might be suitable to study the crack propagation behavior (Liu et al. 2018). After the crack initiation, there is a good agreement between the developed theory for a propagating crack and the FEM simulation in Liu et al. (2018); this is the major focus of this work - to develop a theory for cracks propagating along elastic interfaces. Also note that Eq. (3) was verified by local FEM methods such as the cohesive zone model (CZM) and virtual crack closure technique (VCCT) in Chen et al. (2020b) for a stationary crack. Further discussion of the local and nonlocal FEM methods is beyond the scope of this study.

2. Numerical verification for DCBs under 10.0 m s$^{-1}$ opening rate

The theoretical solution of dynamic ERR for the DCB test under 10.0 m s$^{-1}$ opening rate is plotted against time in Fig. 5 with the corresponding crack length from Liu et al. (2018) plotted on the secondary axis.

It is seen in Fig. 5 that the analytical solution is in good agreement with results from the FEM as expected. But a slightly higher dynamic ERR is with the analytical solution due to the reasons discussed. The relative difference of the CIT values from the developed theory and FEM simulation is 27.5% for the crack initiation.

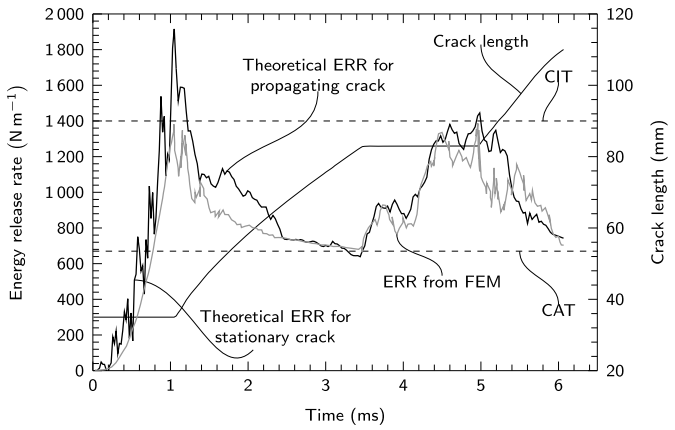


**Fig. 4.** Evolution of dynamic ERR and crack length for 6.5 m s$^{-1}$ opening rate based on FEM results for crack length and crack propagating speed using analytical solution for elastic interface.

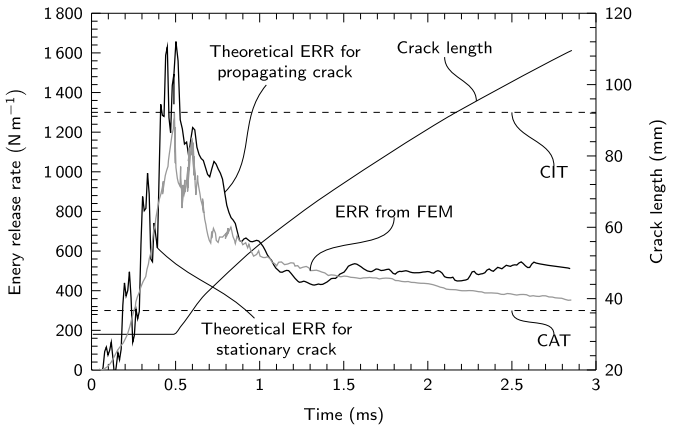


**Fig. 5.** Evolution of dynamic ERR and crack length for 10.0 m s$^{-1}$ opening rate based on FEM results for crack length and crack propagating speed using analytical solution for elastic interface.

The two verifications show an excellent agreement of the ERR predicted by the developed theory and the results from FEM simulations (Liu et al. 2018) for a propagating crack. Before the crack initiation and for the CIT value, a discrepancy is seen between the two methods, and the possible reasons for this were examined: (1) a stiffer analytical model, compared to the FEM model, and (2) the local assessment of crack initiation in the analytical model in contrast to a nonlocal treatment of fracture in the FEM model.

## Conclusion

The dynamic mode-I ERR of cracks propagating along a linear elastic interface in a symmetric DCB is derived with accounting for structural vibration, wave propagation, and the Doppler effect along with the assumption of crack tip energy conservation. Considering the beams as highly dispersive waveguides, a correction factor for dispersion is derived as an average of two limiting boundary conditions to assess the energy supplied to the crack tip for crack growth. In addition, one new method of compliance calibration for the determination of foundation stiffness is derived and presented alongside an alternative method from the authors' previous work.

The developed theory is then verified against FEM simulations of two experimental cases from the literature, demonstrating the excellent ability of the developed theory to capture crack propagating behaviors such as initiation, propagation, arrest, and reinitiation. These crack propagating behaviors are related to the CIT and CAT values, indicating that the developed theory can be applied to measure the CIT and CAT values for CFRPs and adhesives.

To the best of the authors' knowledge, this work presents the analytical solutions of dynamic ERR for propagating cracks on linear elastic interfaces for the first time. Since the analytical solution can be used to study the fracture behavior as well as to measure CIT and CAT values, they are expected to be useful to both engineers and researchers working with layered materials, joints, and bonds to predict dynamic fracture behavior and to determine interface material properties.

## Appendix I. Derivation of Deflections

The deflections of the foundation-supported and free beam sections are derived by solving the governing equations (Rao 2007)

$$EIw^{(4)}(x,t) + \rho A\ddot{w}(x,t) + kw(x,t) = 0 \tag{13}$$

$$EIw^{(4)}(x,t) + \rho A\ddot{w}(x,t) = 0 \tag{14}$$

Since the beam system is under the time-dependent boundary condition, Grant's method (Grant 1983) is employed by introducing the shifting functions, and deflections of respective beam sections take the following form:

$$w^{\mathrm{FD}}(x,t) = w_{\mathrm{fv}}^{\mathrm{FD}}(x,t) + F^{\mathrm{FD}}(x)vt \tag{15}$$

and

$$w^{\mathrm{FR}}(x,t) = w_{\mathrm{fv}}^{\mathrm{FR}}(x,t) + F^{\mathrm{FR}}(x)vt \tag{16}$$

where $w_{\mathrm{fv}}^{\mathrm{FD}}(x,t)$ and $w_{\mathrm{fv}}^{\mathrm{FR}}(x,t)$ are the free-vibration components; and $F^{\mathrm{FD}}(x)$ and $F^{\mathrm{FR}}(x)$ are the shifting functions.

Therefore, combining Eqs. (13) and (15) and forcing the homogeneous conditions, the governing equations for the free-vibration component of the foundation-supported beam section and the shifting functions are derived

$$EIw_{\mathrm{fv}}^{\mathrm{FD}(4)}(x,t) + \rho A\ddot{w}_{\mathrm{fv}}^{\mathrm{FD}}(x,t) + kw_{\mathrm{fv}}^{\mathrm{FD}}(x,t) = 0 \tag{17}$$

$$EIF^{\mathrm{FD}(4)}(x) + kF^{\mathrm{FD}}(x) = 0 \tag{18}$$

Similarly, the governing equations for the free-vibration component of the free beam section and the corresponding shifting functions by combining Eqs. (14) and (16) are

$$EIw_{\mathrm{fv}}^{\mathrm{FR}(4)}(x,t) + \rho A\ddot{w}_{\mathrm{fv}}^{\mathrm{FR}}(x,t) = 0 \tag{19}$$

$$F^{\mathrm{FR}(4)}(x) = 0 \tag{20}$$

## Appendix II. Solutions of Free-Vibration Components

By the method of separation of variables, the solutions for $w_{\mathrm{fv}}^{\mathrm{FD}}(x,t)$ and $w_{\mathrm{fv}}^{\mathrm{FR}}(x,t)$ in Eqs. (17) and (19) are

$$w_{\mathrm{fv}}^{\mathrm{FD}}(x,t) = \sum_{i=1}^{\infty} W_i^{\mathrm{FD}}(x)T_i(t) \tag{21}$$

$$w_{\mathrm{fv}}^{\mathrm{FR}}(x,t) = \sum_{i=1}^{\infty} W_i^{\mathrm{FR}}(x)T_i(t) \tag{22}$$

where $W_i^{\mathrm{FD}}(x)$ and $W_i^{\mathrm{FR}}(x)$ are the $i$th normal mode for the foundation-supported and free beam sections, respectively; and $T_i(t)$ is the time-dependent modal displacement of the $i$th normal mode.

Combining the boundary conditions and introducing natural frequency $\omega_i$ together with wavenumbers $\alpha_i$ and $\beta_i$, the $i$th normal modes for the foundation-supported and free beam sections as well as the modal displacement are

$$W_i^{\mathrm{FD}}(x) = C_{i1}[\cosh(\alpha_i x)\sin(\alpha_i x) - \sinh(\alpha_i x)\cos(\alpha_i x)] + C_{i2}\sinh(\alpha_i x)\sin(\alpha_i x) \tag{23}$$

$$W_i^{\mathrm{FR}}(x) = C_{i3}\sinh[\beta_i(x-L-a)] + C_{i4}\sin[\beta_i(x-L-a)] \tag{24}$$

$$T_i(t) = T_i(0)\cos(\omega_i t) + \frac{\dot{T}_i(0)}{\omega_i}\sin(\omega_i t) \tag{25}$$

where $C_{i1}$, $C_{i2}$, $C_{i3}$, and $C_{i4}$ are coefficients to be determined by the boundary and orthogonality conditions in Eq. (26); $\alpha_i$ and $\beta_i$ are $4\alpha_i^4 = k/(EI) - \omega_i^2\rho A/(EI)$ and $\beta_i^4 = \omega_i^2\rho A/(EI)$; and $T_i(0)$ and $\dot{T}_i(0)$ are the initial modal displacement and velocity, respectively

$$\int_0^L \rho A W_i^{\mathrm{FD}}(x)W_j^{\mathrm{FD}}(x)dx + \int_L^{L+a} \rho A W_i^{\mathrm{FR}}(x)W_j^{\mathrm{FR}}(x)dx = \delta_{ij} \tag{26}$$

By applying the continuity condition at the crack tip, $x = L$, the following system of equations is derived:

$$\begin{bmatrix} \begin{pmatrix} \cosh(\alpha_i L)\sin(\alpha_i L) \\ -\sinh(\alpha_i L)\cos(\alpha_i L) \end{pmatrix} & \sinh(\alpha_i L)\sin(\alpha_i L) & \sinh(\beta_i a) & \sin(\beta_i a) \\ 2\alpha_i \sinh(\alpha_i L)\sin(\alpha_i L) & \alpha_i \begin{pmatrix} \sinh(\alpha_i L)\cos(\alpha_i L) \\ +\cosh(\alpha_i L)\sin(\alpha_i L) \end{pmatrix} & -\beta_i \cosh(\beta_i a) & -\beta_i \cos(\beta_i a) \\ 2\alpha_i^2 \begin{pmatrix} \sinh(\alpha_i L)\cos(\alpha_i L) \\ +\cosh(\alpha_i L)\sin(\alpha_i L) \end{pmatrix} & 2\alpha_i^2 \cosh(\alpha_i L)\cos(\alpha_i L) & \beta_i^2 \sinh(\beta_i a) & -\beta_i^2 \sin(\beta_i a) \\ 4\alpha_i^3 \cosh(\alpha_i L)\cos(\alpha_i L) & 2\alpha_i^3 \begin{pmatrix} \sinh(\alpha_i L)\cos(\alpha_i L) \\ -\cosh(\alpha_i L)\sin(\alpha_i L) \end{pmatrix} & -\beta_i^3 \cosh(\beta_i a) & \beta_i^3 \cos(\beta_i a) \end{bmatrix} \begin{pmatrix} C_{i1} \\ C_{i2} \\ C_{i3} \\ C_{i4} \end{pmatrix} = \begin{pmatrix} 0 \\ 0 \\ 0 \\ 0 \end{pmatrix} \tag{27}$$

For this homogeneous system of linear equations to have nonzero solutions, the determinant of the coefficient matrix must be zero. Let $D_i$ be the determinant of the coefficient matrix of Eq. (27). From $D_i = 0$, the wavenumbers $\alpha_i$ and $\beta_i$ can be determined and, thus, the natural frequency $\omega_i$ via $4\alpha_i^4 = k/(EI) - \omega_i^2 \rho A/(EI)$ or $\beta_i^4 = \omega_i^2 \rho A/(EI)$.

As for the initial values of the $i$th modal displacement and velocity, it is found that $T_i(0) = 0$ and

$$\dot{T}_i(0) = -vH_i \tag{28}$$

where $H_i = \int_0^L \rho A W_i^{\mathrm{FD}}(x) F^{\mathrm{FD}}(x)dx + \int_L^{L+a} \rho A W_i^{\mathrm{FR}}(x) F^{\mathrm{FR}}(x)dx$.

## Appendix III. Solutions of Shifting Functions

The shifting functions are obtained by solving governing equations Eqs. (18) and (20), giving

$$F^{\mathrm{FD}}(x) = P_1[\cosh(\gamma x)\sin(\gamma x) - \sinh(\gamma x)\cos(\gamma x)] + P_2 \sinh(\gamma x)\sin(\gamma x) \tag{29}$$

$$F^{\mathrm{FR}}(x) = P_3(x - L - a)^3 + P_4(x - L - a) + 1 \tag{30}$$

where the coefficients $P_1$, $P_2$, $P_3$, and $P_4$ are

$$P_1 = \frac{-6[\cosh(\gamma L)\cos(\gamma L) + a\gamma \sinh(\gamma L)\cos(\gamma L) - a\gamma \cosh(\gamma L)\sin(\gamma L)]}{P_0} \tag{31}$$

$$P_2 = \frac{-6[\sinh(\gamma L)\cos(\gamma L) + \cosh(\gamma L)\sin(\gamma L) + 2a\gamma \cosh(\gamma L)\cos(\gamma L)]}{P_0} \tag{32}$$

$$P_3 = \frac{-\gamma^3[\cosh(2\gamma L) + \cos(2\gamma L) + 2]}{P_0} \tag{33}$$

$$P_4 = \frac{3\gamma\{a^2\gamma^2[\cosh(2\gamma L) + \cos(2\gamma L) + 2] + 2a\gamma[\sinh(2\gamma L) + \sin(2\gamma L)] + [\cosh(2\gamma L) - \cos(2\gamma L)]\}}{P_0} \tag{34}$$

with $P_0 = \{2a^3\gamma^3[\cos(2\gamma L) + \cosh(2\gamma L) + 2] + 6a^2\gamma^2[\sin(2\gamma L) + \sinh(2\gamma L)] + 6a\gamma[\cosh(2\gamma L) - \cos(2\gamma L)] + 3[\sinh(2\gamma L) - \sin(2\gamma L)]\}$.

Note that for the product of the foundation stiffness $k$ and the length of the foundation-supported beam section L is large enough to satisfy $\tanh(2\gamma L) \approx 1$ (that is, $\gamma L \gtrapprox 3$ so that $\tanh(6) \approx 0.999999$), $P_3$ in Eq. (33) approximates to

$$P_3 = \frac{-\gamma^3}{2a^3\gamma^3 + 6a^2\gamma^2 + 6a\gamma + 3} \tag{35}$$

## Appendix IV. Derivation of Energy Release Rate

Combining the results from Appendixes I to IV, the total deflections of the foundation-supported and free beam sections are given in Eqs. (1) and (2), respectively. These deflections provide the total mechanical energy $\Pi = \Pi_{\mathrm{st}}^{\mathrm{U}} + \Pi_{\mathrm{vib}} + \Pi_{\mathrm{st}}^{\mathrm{K}}$, where $\Pi_{\mathrm{st}}^{\mathrm{U}}$ is the strain energy component due to static motion, $\Pi_{\mathrm{st}}^{\mathrm{K}}$ is the kinetic energy component due to static motion, and $\Pi_{\mathrm{vib}}$ is the vibrating energy component

$$\Pi_{\mathrm{st}}^{\mathrm{U}} = -\frac{1}{2} EI v^2 t^2 F^{\mathrm{FR}(3)}(L + a) \tag{36}$$

$$\Pi_{\mathrm{st}}^{\mathrm{K}} = \frac{1}{2}\rho A \int_0^L [F^{\mathrm{FD}}(x)v]^2 dx + \frac{1}{2}\int_L^{L+a} [F^{\mathrm{FR}}(x)v]^2 dx \tag{37}$$

$$\Pi_{\mathrm{vib}} = -v^2 \sum_{i=1}^{\infty} H_i^2 \cos(\omega_i t) + \frac{1}{2} v^2 \sum_{i=1}^{\infty} H_i^2 \tag{38}$$

Correspondingly, the ERR components due to each energy term above are

$$G_{\mathrm{st}}^{\mathrm{U}} = -\frac{d\Pi_{\mathrm{st}}^{\mathrm{U}}}{bda} = \frac{9EI v^2 t^2 f_{\mathrm{st}}^{\mathrm{U}}}{2ba^4} \tag{39}$$

where $f_{\mathrm{st}}^{\mathrm{U}} = 4a^4\gamma^4(a\gamma + 1)^2/(2a^3\gamma^3 + 6a^2\gamma^2 + 6a\gamma + 3)^2$

$$G_{\mathrm{st}}^{\mathrm{K}} = -\frac{d\Pi_{\mathrm{st}}^{\mathrm{K}}}{bda} = -\frac{33\rho A v^2 f_{\mathrm{st}}^{\mathrm{K}}}{280b} \tag{40}$$

which is found to be small compared to the other ERR components and can be omitted; and

$$G_{\mathrm{vib}} = \frac{F_{\mathrm{vib}}(\Omega)}{b\dot{a}} = \frac{v^2 t}{2b}\sum_{i=1}^{\infty}(-1)^i\sqrt{\frac{\omega_1}{\omega_i}}H_i^2\frac{d\omega_i}{da}\sin(\omega_i t) \tag{41}$$

which is derived by Freund's energy flux method as well as a consideration of flexural wave propagation in beams as dispersive waveguides, and where

$$\frac{d\omega_i}{da} = 2\beta_i\left(\frac{\partial D_i}{\partial L} - \frac{\partial D_i}{\partial a}\right)\sqrt{\frac{EI}{\rho A}}\Bigg/\left(-\frac{\partial D_i}{\partial \alpha_i}\frac{\beta_i^3}{4\alpha_i^3} + \frac{\partial D_i}{\partial \beta_i}\right) \tag{42}$$

where $D_i$ is the determinant of coefficient matrix of Eq. (27).

Therefore, combining results from Appendixes I to IV, the ERR is obtained as shown in Eq. (3)

## Data Availability Statement

Some or all data, models, or code that support the findings of this study are available from the corresponding author upon reasonable request.

## Acknowledgments

This work was supported by the National Natural Science Foundation of China (Grant Nos. 51401028, 51271193, and 11790292), the Strategic Priority Research Program of the Chinese Academy of Sciences (Grant No. XDB22040303), and the Innovation Program (237099000000170004).

## Notation

*The following symbols are used in this paper:*

$A$ = area of cross section of beam section;
$a$ = crack length;
$\dot{a}$ = crack propagating speed;
$b$ = width of beam;
$C_{\mathrm{g}}^i$ = group speed of the $i$th mode flexural wave;
$C_{\mathrm{p}}^1$ = phase speed of the $i$th mode flexural wave;
$E$ = Young's modulus;
$F^{\mathrm{FD}}(x)$ = shifting function for foundation-supported beam section;
$F^{\mathrm{FR}}(x)$ = shifting function for free beam section;
$G$ = total energy release rate;
$G_{\mathrm{vib}}$ = ERR component due to vibration;
$G_{\mathrm{st}}^{\mathrm{U}}$ = ERR component due to the strain energy of quasi-static motion;
$h$ = thickness of beam;
$I$ = second moment of area of beam section;
$L$ = length of foundation-supported beam section;
$t$ = time;
$v$ = applied constant displacement rate;
$w^{\mathrm{FD}}(x,t)$ = deflection for foundation-supported and free beam section;
$W_i^{\mathrm{FD}}(x)$ = $i$th normal mode for foundation-supported beam section;
$w^{\mathrm{FR}}(x,t)$ = deflection for free beam section;
$W_i^{\mathrm{FR}}(x)$ = $i$th normal mode for free beam section;
$\alpha_i$ = wavenumber for foundation-supported beam section;
$\beta_i$ = wavenumber for free beam section;
$\nu$ = Poisson's ratio;
$\rho$ = density; and
$\omega_i$ = angular frequency of the $i$th vibration mode.

## References

ASTM. 2015. *Standard test method for tensile properties of plastics*. ASTM D638. West Conshohocken, PA: ASTM.

ASTM. 2016. *Standard test method for mode I interlaminar fracture toughness of unidirectional fiber-reinforced polymer matrix composites*. ASTM D5528. West Conshohocken, PA: ASTM.

Blackman, B. R. K., J. P. Dear, A. J. Kinloch, H. Macgillivray, Y. Wang, J. G. Williams, and P. Yayla. 1995. "The failure of fibre composites and adhesively bonded fibre composites under high rates of test—Part I: Mode I loading-experimental studies." *J. Mater. Sci.* 30 (23): 5885–5900. https://doi.org/10.1007/BF01151502.

Blackman, B. R. K., A. J. Kinloch, Y. Wang, and J. G. Williams. 1996. "The failure of fibre composites and adhesively bonded fibre composites under high rates of test—Part II: Mode I loading-dynamic effects." *J. Mater. Sci.* 31 (17): 4451–4466. https://doi.org/10.1007/BF00366341.

Chen, T., C. M. Harvey, S. Wang, and V. V. Silberschmidt. 2020a. "Delamination propagation under high loading rate." *Compos. Struct.* 253 (Dec): 112734. https://doi.org/10.1016/j.compstruct.2020.112734.

Chen, T., C. M. Harvey, S. Wang, and V. V. Silberschmidt. 2020b. "Dynamic delamination on elastic interface." *Compos. Struct.* 234 (Feb): 111670. https://doi.org/10.1016/j.compstruct.2019.111670.

Chen, T., C. M. Harvey, S. Wang, and V. V. Silberschmidt. 2020c. "Dynamic interfacial fracture of a double cantilever beam." *Eng. Fract. Mech.* 225 (Feb): 106246. https://doi.org/10.1016/j.engfracmech.2018.11.033.

Chen, T., C. M. Harvey, S. Wang, and V. V. Silberschmidt. 2020d. "Theory of dynamic mode-II delamination in end-loaded split tests." *Composites, Part C: Open Access* 3 (Nov): 100055. https://doi.org/10.1016/j.jcomc.2020.100055.

Chen, T., C. M. Harvey, S. Wang, and V. V. Silberschmidt. 2021a. "Analytical corrections for double-cantilever beam tests." *Int. J. Fract.* 229 (2): 269–276. https://doi.org/10.1007/s10704-021-00556-5.

Chen, T., C. M. Harvey, S. Wang, and V. V. Silberschmidt. 2021b. "Theory of dynamic mode-II delamination in end-notched flexure tests." *Compos. Struct.* 274 (Oct): 114332. https://doi.org/10.1016/j.compstruct.2021.114332.

Davidson, P., and M. W. Anthony. 2012. "Non-smooth mode I fracture of fibre-reinforced composites: An experimental, numerical and analytical study." *Philos. Trans. R. Soc. London, Ser. A* 370 (1965): 1942–1965. https://doi.org/10.1098/rsta.2011.0381.

Davidson, P., M. W. Anthony, and C. S. Yerramalli. 2012. "Experimental determination of validated, critical interfacial modes I and II energy release rates in a composite sandwich panel." *Compos. Struct.* 94 (2): 477–483. https://doi.org/10.1016/j.compstruct.2011.08.007.

Freund, L. B. 1990. *Dynamic fracture mechanics*. Cambridge, UK: Cambridge University Press.

Friedrich, K., R. Walter, L. A. Carlsson, A. J. Smiley, and J. W. Gillespie. 1989. "Mechanisms for rate effects on interlaminar fracture toughness of carbon/epoxy and carbon/PEEK composites." *J. Mater. Sci.* 24 (9): 3387–3398. https://doi.org/10.1007/BF01139070.

Grant, D. A. 1983. "Beam vibrations with time-dependent boundary conditions." *J. Sound Vib.* 89 (4): 519–522. https://doi.org/10.1016/0022-460X(83)90353-X.

Hashemi, S., A. J. Kinloch, and J. G. Williams. 1989. "Corrections needed in double-cantilever beam tests for assessing the interlaminar failure of fibre-composites." *J. Mater. Sci. Lett.* 8 (2): 125–129. https://doi.org/10.1007/BF00730701.

ISO. 2009. *Adhesives—Determination of the mode 1 adhesive fracture energy of structural adhesive joints using double cantilever beam and tapered double cantilever beam specimens*. ISO 25217. Geneva: ISO.

ISO. 2019. *Plastics—Determination of tensile properties*. ISO 527. Geneva: ISO.
Kanninen, M. F. 1974. "A dynamic analysis of unstable crack propagation and arrest in the DCB test specimen." *Int. J. Fract.* 10 (3): 415–430. https://doi.org/10.1007/BF00035502.
Kanninen, M. F., C. Popelar, and P. C. Gehlen. 1977. *Dynamic analysis of crack propagation and arrest in the DCB specimen*. ASTM Special Technical Publication 627. West Conshohocken, PA: ASTM.
Liu, Y., F. P. van der Meer, and L. J. Sluys. 2018. "Cohesive zone and interfacial thick level set modeling of the dynamic double cantilever beam test of composite laminate." *Theor. Appl. Fract. Mech.* 96 (Aug): 617–630. https://doi.org/10.1016/j.tafmec.2018.07.004.
Rao, S. S. 2007. *Vibration of continuous systems*. Hoboken, NJ: Wiley.
Smiley, A. J., and R. B. Pipes. 1987. "Rate effects on mode I interlaminar fracture toughness in composite materials." *J. Compos. Mater.* 21 (7): 670–687. https://doi.org/10.1177/002199838702100706.
Sun, C., M. D. Thouless, A. M. Waas, J. A. Schroeder, and P. D. Zavattieri. 2008. "Ductile-brittle transmissions in the fracture of plastically-deforming, adhesively-bonded structures. Part I: Experimental studies." *Int. J. Solids Struct.* 45 (10): 3059–3073. https://doi.org/10.1016/j.ijsolstr.2008.01.011.